Carbon Dioxide Adsorption in Amine-Functionalized Mixed-Ligand Metal-Organic Frameworks of UiO-66 Topology

J. Ethiraj,E. Albanese,B. Civalleri,J. G. Vitillo,F. Bonino,S. Chavan,G. C. Shearer,K. P. Lillerud,S. Bordiga
Carbon Dioxide Adsorption in Amine-Functionalized Mixed-Ligand Metal-Organic Frameworks of UiO-66 Topology
CHEMSUSCHEM (2014) 7
DOI: 10.1002/cssc.201402694

CO_2 Adsorption in Amine Functionalized Mixed Ligand Metal-organic Frameworks of UiO-66 topology

Jayashree Ethiraj,[a] Elisa Albanese,[a] Bartolomeo Civalleri,[a] Jenny G. Vitillo,*[a,c] Francesca Bonino,*[a] Sachin Chavan,[b] Greig C. Shearer,[b] Karl Petter Lillerud,[b] Silvia Bordiga,[a]

Abstract: A series of mixed ligand (ML: H_2-BDC/NH_2-BDC) UiO-66 MOFs, synthesized via two different methods (LT, low temperature and HT, high temperature) have been investigated for their CO_2 adsorption properties from 0 to 1 bar in order to clarify the role of NH_2 loading on CO_2 uptake. Volumetric CO_2 isotherms show that the CO_2 capacity (normalized to the Langmuir surface area) increases with the functionalization degree of about 46%; for similar NH_2 content same values are found for both the synthesis procedures. Microcalorimetric isotherms reveal that amino-functionalized materials have a larger differential heat of adsorption (q^{diff}) towards CO_2; respectively reaching 27 (25) and 20 (22) kJ/mol on HT(LT) UiO-66-NH_2 and UiO-66 at the lowest equilibrium pressures used in this study. All experimental results are well supported by values obtained via quantum mechanical calculations.

Introduction

The trend of CO_2 emissions in the atmosphere mainly reflects energy related human activities which, over the past decade, were determined by economic growth, particularly in developing countries. These emissions, which stem predominantly from the combustion of coal, oil, and natural gas are projected to continue to increase in the future due to economic growth and industrial development.[1] Many research efforts are being made to improve the performance of materials in CO_2 separation from flue gases and storage.[2-5] To this end, metal organic frameworks (MOFs) constitute a class of materials of particular interest due to their high porosity and the ease at which to their surface chemistry can be modified via the incorporation of performance enhancing chemical functionalities (such as amines). [3, 6-10]

With the aim of the rational design of new high capacity MOFs, the interaction between CO_2 and aliphatic and aromatic amines has been studied by quantum mechanical methods, focusing attention on as yet unutilized amine-based linkers as well as previously reported systems. [11, 12]

UiO-66[13-16] is a Zr(IV)-based MOF that has recently received great interest due to its high thermal and chemical stability. Many examples in the literature illustrate the potential of the material in sorption applications. Wu et al. [17] reported that the systematic use of a modulator such as acetic acid induces missing-linker defects into the framework, leading to greatly improved porosity and thus gas uptake. UiO-66 has been synthesized with many different organic functionalities on the linkers, generating an isoreticular series of UiO-66-X MOFs (X = F, Cl, Br, I, CH_3, $(CH_3)_2$, $(CF_3)_2$, NO_2, NH_2, OH, $(OH)_2$, OCH_3, SO_3H, C_6H_4).[7, 18] NH_2-functionalised UiO-66 MOFs have shown increased CO_2 uptake with respect to the unfunctionalized material at 1 bar [19]. Furthermore, photocatalytic CO_2 reduction has been reported on UiO-66-NH_2 and its derivatives [20]. Herein, we focus our attention on UiO-66-NH_2, and investigate the effect of NH_2 loading on the CO_2 adsorption performance. To this end, an isostructural series of mixed ligand (ML) UiO-66 MOFs with NH_2 content ranging from 0 to 100% of the linkers were successfully synthesized and have previously been deeply characterized by Chavan et al. in Ref. [8]. The materials have been studied for their potential in CO_2 adsorption via a multi-technique approach involving FTIR spectroscopy, adsorption/desorption isotherms and microcalorimetric measurements. Periodic quantum mechanical calculations have also been performed in order to gain fundamental insight.

Results and Discussion

For the two series of samples, preliminary FT-IR studies on the best activation temperature (under vacuum) have been performed. In particular, the aim was to identify the minimum temperature at which all residual solvent (H_2O and traces of DMF) could be removed while preserving the majority of the structural hydroxyl groups on the LT/HT UiO-66 samples. All other samples were then subjected to the same treatment. The required activation conditions were in fact different depending on the synthesis method used: 393 K for 2 h for the LT samples and 423 K for 1 h for the HT samples.

The FT-IR spectra recorded on activated LT-ML-MOFs and HT-ML-MOFs are reported in Figure 1a) and 1b) respectively. A very intense band at 3673 cm^{-1} can be observed in all spectra, previously assigned to the hydroxyl groups on the inorganic cornerstones of the materials.[15, 36] The intensity of this band is observed to decrease with increasing ABDC (2-amino-1,4-

[a] J. Ethiraj, Dr. E. Albanese, Dr. B. Civalleri, Prof. S. Bordiga, Dr. J. G. Vitillo, Dr. F. Bonino
Department of Chemistry,
NIS and INSTM Reference Centre,
University of Turin,
Via G. Quarello 15, I-10135 and Via P. Giuria 7, I-10125, Turin, Italy
E-mail: Francesca.bonino@unito.it
[b] Dr. S. Chavan, G.C. Shearer, Prof. K.P. Lillerud,
Department of Chemistry,
inGAP centre of Research-based Innovation,
University of Oslo, SemSælandsvei 26, N-0315 Oslo, Norway
[c] Dr. J. G. Vitillo
Dipartimento di Scienza ed Alta Tecnologia,
Università degli Studi dell'Insubria, Via Lucini 3, I-22100-Como, Italy

Supporting information for this article is given via a link at the end of the document.((Please delete this text if not appropriate))

benzenedicarboxylic acid) content, as clearly shown on the inset of Figure 1a, where the spectra obtained on LT-UiO-66 and LT-UiO-66-NH_2 are compared.

Focusing attention on the spectra recorded on the LT-ML-MOFs (Figure 1a), the intensity of the asymmetric and symmetric N-H stretching bands ,appearing at 3518 cm^{-1} and 3404 cm^{-1}respectively, can clearly be seen to systematically increase with the amino content of the samples. These two bands are blue shifted with respect to those observed on the free ABDC ligand (3508 cm^{-1} and 3393 cm^{-1}).[7] This means that the –NH_2 groups in the MOFs undergo hydrogen bonding to a lesser extent than those in pure ABDC. Interestingly, a shoulder at 3328 cm^{-1} is clearly visible only on the spectra recorded on the LT-ML-MOF series of samples.

At lower (1800-900 cm^{-1}) vibrational frequencies, the spectra of the amino-modified materials feature additional bands with respect to the unfunctionalised material at 1707, 1656, 1628, 1339, 1254 cm^{-1}, close to the range of OCO carboxylate asymmetric and symmetric stretching modes (1650-1350 cm^{-1})[15, 31] and at 1127 and 968 cm^{-1}. Some of these bands feature in the FTIR spectrum simulated from the model UiO-66-NH_2-50 structure (see Supporting Information). The intensity of all these bands increases in proportion to the NH_2 content of the samples. Conversely, the very sharp and intense band at 1019 cm^{-1} is progressively eroded with increasing amino content. This band is assigned to one of the benzene ring C-H deformation modes and is particularly active when NH_2 functionality is absent.[15] DRIFTs results previously reported by Chavan et al. [8] confirm some of these observations.

The same qualitative changes to the MOF spectra with NH_2 content is also observed on the HT-ML-MOFs (part b of Figure 1). However, the NH_2 stretching bands appear at the lower frequencies of 3495 and 3387 cm^{-1}, respectively, such that they are red shifted with respect to the free ABDC linker. Furthermore, their FWHM (Full Width at Half Maximum) increases such that the observation of the low frequency shoulder is obscured. At frequencies higher than carboxylate OCO stretching modes (1650-1350 cm^{-1})[15], only a single shouldering band is present, while at lower frequencies, bands centered at 1339, 1254, 1127 and 968 cm^{-1} are observed. The erosion of the benzene ring C-H deformation band at 1019 cm^{-1} is also observed in this HT-ML-MOF series.

The IR spectrum simulated from an idealized model of UiO-66-NH_2-50 is reported in the Supporting Information and is compared with LT-UiO-66-NH_2-57, showing a good agreement (see Figure S1).

It is well known that even when CO_2 interacts with very strong sites, neither its asymmetric nor its symmetric stretching mode are significantly perturbed.[7, 11, 31, 37, 38] The results obtained in this study are no exception, as the CO_2 spectra obtained on all of the materials under study were almost identical to those obtained on LT-UiO-66-NH_2, reported in Figure S2b.

Furthermore, the very weak interaction of CO_2 with the NH_2 and OH groups is confirmed by the fact that their respective stretching modes are completely unperturbed, even at the highest CO_2 dosage (see Figure S2a). These findings were fully confirmed by the calorimetric measurements.

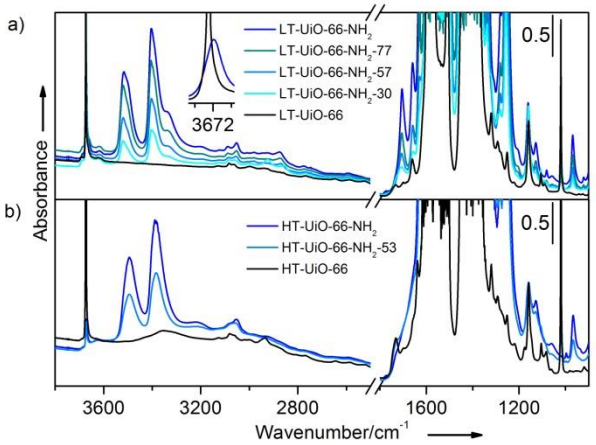

Figure 1. FT-IR spectra of activated a) LT-ML-MOFs and b) HT-ML-MOFs.

Volumetric CO_2 isotherms recorded at 298 K in the 0-1 bar pressure range are reported in Figure 2, where results obtained on the LT-ML-MOFs (part a) and HT-ML-MOFs (part b) are shown. Both the LT and HT series of samples show the same qualitative behavior. However, because of their larger surface area (see Table 1), all the materials synthesized at low temperature (cost-efficient synthesis) attain a higher CO_2 capacity than the corresponding materials synthesized at high temperature. The structural integrity of all the samples after CO_2 volumetric isotherms has been verified by PXRD (see Figure S4 in the Supporting Information). On both series of samples, a coincidence of the adsorption and desorption curves is observed within the error scale of the measurements (about 10% of the adsorbed amounts), indicating that the process is completely reversible. This is in agreement with our IR measurements and with previous volumetric studies conducted on UiO-66 and UiO-66-NH_2 at higher pressures (up to 50 bar).[39] The low adsorbate-adsorbent interaction energy is particularly evident when considering the shape of the curves, where it can be seen that adsorption is far from saturation at 1 bar, (saturation is eventually reached at pressures above 10 bar).[10, 40] Nevertheless, it is evident as the affinity toward CO_2 increases with the NH_2 content. In Table 1, the CO_2 capacities of these materials (1 bar, RT) are compared with the theoretical maximum capacities (estimated on the basis of the microporous volume of the material and the density of liquid CO_2). It was found that the measured CO_2 uptakes at 298 K and 1 bar (1.99-3.04 mol CO_2/kg) are significantly lower than the theoretically maximum loading (6.65-8.28 mol CO_2/kg, see Table 1). These values are reached only at high pressures (> 10 bar) as determined in previous studies on UiO-66 and UiO-66-NH_2.[40] It is noteworthy that the relative order of the CO_2 capacities at 1 bar is inverse with respect to what is expected on the basis of the micropore volume and surface area of the samples, and that the uptake instead increases with the NH_2 content in the samples. Such an increase of low pressure CO_2 capacity upon amino-functionalisation has been already reported for other MOFs, e.g. MIL-53(Al).[3]

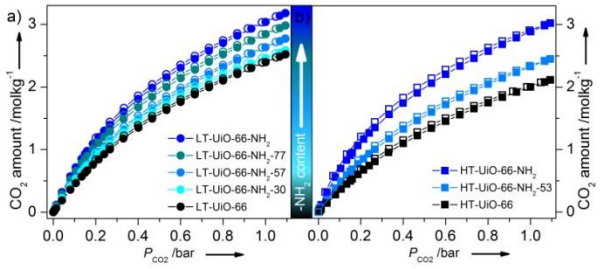

Figure 2. Excess CO_2 adsorption isotherms at 298K obtained on a) LT-ML-MOFs and b) HT-ML-MOFs. Adsorption and desorption curves are displayed as filled and empty symbols respectively.

To better understand the effect of the extent of NH_2 functionality on the CO_2 capacity at 1 bar, Figure 3 displays the results obtained when the CO_2 uptake is normalized to the Langmuir surface areas of the materials. The plot effectively demonstrates that the same amount of CO_2 is adsorbed on materials with the same NH_2 content (within the error of the measurements), independent of the synthesis procedure used. Another important observation is that at ABDC contents above 50%, the affinity of the materials for CO_2 strongly increases (compare the slope of the curve in the 0-50% and 50-100% NH_2 ranges). This larger affinity can be explained by the larger probability of having adjacent -NH_2 sites in the material at higher ABDC loadings. Such sites have previously been predicted to be advantageous to the CO_2 adsorption energy.[11]

Table 1. Textural properties* and CO_2 capacities of ML-MOFs.

ML-MOFs	S_{BET} (m^2/g) [a]	$S_{Langmuir}$ (m^2/g) [b]	V_m (cm^3/g) [c]	CO_2 capacity at 1 bar (mol/kg)	Maximal CO_2 capacity (mol/kg) [d]
LT-UiO-66	1331	1444	0.47	2.39	8.28
LT-UiO-66-NH_2-30	1284	1378	0.46	2.45	7.98
LT-UiO-66-NH_2-57	1252	1361	0.44	2.63	7.78
LT-UiO-66-NH_2-77	1198	1298	0.43	2.84	7.45
LT-UiO-66-NH_2	1161	1254	0.41	3.04	7.17
HT-UiO-66	1170	1272	0.42	1.99	7.17
HT-UiO-66-NH_2-53	1139	1216	0.40	2.33	7.00
HT-UiO-66-NH_2	1057	1130	0.38	2.89	6.65

[a] Area evaluated following the BET. [b] Langmuir model. [c] Micropore volume as reported in Ref.[8]. [d] Capacity estimated from the micropore volume, considering the density of liquid CO_2 (770 kg/m^3).
*Theoretical values are reported in the Supporting Information (Figure S3).

CO_2 calorimetric isotherms obtained on UiO-66 and UiO-66-NH_2 (both HT and LT) in the 0-0.1 bar range at 303 K are reported in Figure 4. In this low pressure range, effects of the structural defects present on the LT samples are expected to be more evident.

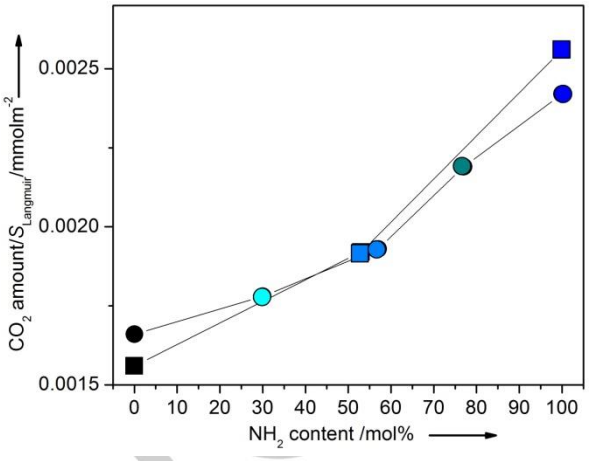

Figure 3. CO_2 capacity at 1 bar (normalized to the Langmuir surface area of the materials) vs. NH_2 content. Circles: LT-ML-MOFs; squares: HT-ML-MOFs.

The volumetric isotherms are reported in Figure 4a and clearly demonstrate Henry-type adsorption because of the low pressure considered. From these curves it is evident that the presence of –NH_2 has an even more dramatic effect on the adsorbed amounts in the 0-0.1 bar range than what was already observed at higher pressure (see Figure 2). In fact, there is 50% increase in the adsorbed amounts in UiO-66-NH_2 when compared to UiO-66, with n_{ads} values of 0.22 μmol/m^2 and 0.34 μmol/m_2 being obtained on HT-UiO-66 and HT-UiO-66-NH_2 respectively. This increase is due to the larger differential heat of adsorption (q^{diff}) on the amino-functionalized materials, as reported in Figure 4c. The q^{diff} recorded at the lowest equilibrium pressures used in this study amount to 27 (25) and 20 (22) kJ/mol on HT(LT)- UiO-66-NH_2 and UiO-66, respectively. These values are in the range expected (12-35 kJ/mol) [3, 40] via comparison with similar systems already reported in the literature, significantly lower than the values reported on aliphatic amine modified MOFs (90-77 kJ/mol),[3] where a chemical reaction may occur. The q^{diff} value obtained on UiO-66-NH_2 is significantly lower than the value of 38.4 kJ/mol reported on amino-MIL-53(Al), whereas the value obtained on unfunctionalized UiO-66 is very close value as that previously found on unfunctionalized MIL-53(Al).[6] The higher affinity of MIL-53-NH_2(Al) is explained by the breathing ability upon adsorption of CO_2, something which does not occur on unfunctionalized MIL-53(Al) or on any materials in the UiO-66 family.[41] The q^{diff} values obtained here on UiO-66 and UiO-66-NH_2 are 7-8 kJ/mol lower than those previously reported by Wiersum et al. for the same systems (27 and 31-35 kJ/mol, respectively).[40] The higher purity and lower defectivity of the samples considered in the present study (for both HT and LT series) with respect to previous works have to be taken into account.[8] Specifically, the S_{BET} reported in ref. [40] on both UiO-66 and UiO-66-NH_2 (970 and 1080 m^2/g, respectively)[40] are considerably lower that their theoretical values (see Supporting Information, Figure S3 for details) in contrast to our values, reported in Table 1. Moreover, the S_{BET} reported in Ref. [40] are in the reverse order to what is theoretically expected (S_{BET} UiO-66 should be higher than S_{BET} UiO-66-NH_2). This is likely

attributable to a large amount of unreacted linkers in the pores of the materials reported in Ref. [40]. Moreover, the previous study found a different dependence of q^{diff} on coverage to that in the present work. That is, q^{diff} is almost constant with coverage in Ref. [40] while it is found to decrease with coverage in this study (Figure 4c). This difference can easily be explained by the vast difference in the pressure range used in the two studies: 0-0.1 bar in the present work and 1-50 bar in ref. [40]. Figure 4c demonstrates that, 3-4 different regimes can be recognized for the dependence of q^{diff} on the coverage in the 0-0.1 bar range: (i) at lower coverages, q^{diff} decreases with increasing n_{ads}; (ii) q^{diff} is constant with increasing n_{ads}; (iii) q^{diff} decreases with increasing n_{ads}; (iv) q^{diff} is constant with increasing n_{ads}. This observation exemplifies the heterogeneous nature of the adsorption sites in the samples studied here. Unfortunately, the identification of the nature of these sites and of their origin can be only speculated on. It is in fact found that different synthetic conditions provide a different dependence of q^{diff} on the coverage. This indicates that the heterogeneity of CO_2 adsorption sites is rooted not only by the presence of different adsorption sites in the structure of the theoretical material but also by the presence of different defect sites that can be further present in the materials.[42]

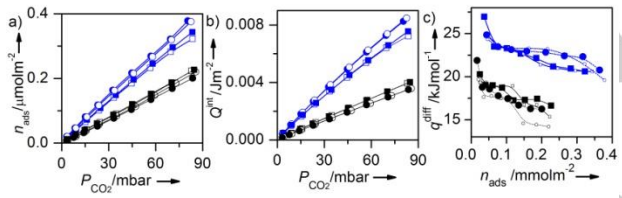

Figure 4. a) CO_2 volumetric and b) calorimetric isotherms obtained at 303K in the 0-0.1 bar range for UiO-66 (black symbols) and UiO-66-NH_2 (blue symbols) materials synthesized at low (circles) and high (squares) temperatures. c) Differential heat q^{diff} distribution obtained from a) and b). The adsorbed amounts (n_{ads}) have been normalised to the Langmuir surface areas. Filled and hollow symbols are used for the primary and secondary adsorption isotherms, respectively.

Both hydroxylated and de-hydroxylated forms of UiO-66-NH_2-50 were modeled. For the de-hydroxylated UiO-66-NH_2-50 model, the interaction of a CO_2 molecule with each of the three amino groups in the unit cell was investigated, corresponding to a 1:1 loading. In the hydroxylated structure, multiple adsorption sites are present. In order to highlight the possible adsorption sites, the Electrostatic Potential (ESP) mapped on top of a charge density isosurface for both hydroxylated and de-hydroxylated forms of UiO-66-NH_2 has been calculated (see Figure 5). In both cases, a localized negative region is observed around the amino groups, while a small but localized positive region is observed on the two different OH groups of the hydroxylated MOF. The ability of these amino groups to polarize incoming probe molecules such as CO_2 is expected to be very low, on the basis of the ESP values obtained. Moreover, the calculations show that they interact with the nearby carboxylate oxygen through hydrogen bonding in the empty material, a fact which is expected to limit the adsorption potential of the amino groups.

According to the ESP plot, three different interaction sites were explored to model the adsorption of CO_2 (see Figure 5): (i) the amino group (site N); (ii) the OH group vicinal to the amino groups (site $OH_{(NH2)}$); (iii) the UiO-66-like OH group (site OH).

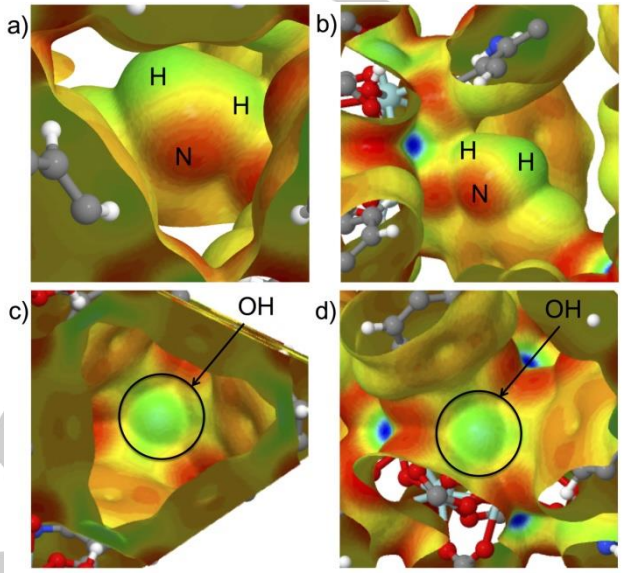

Figure 5. Comparison between the electrostatic potential of UiO-66-NH_2-50 (dehydroxylated and hydroxylated form) mapped on top of a charge density isosurface (0.003 e) for different parts of the structure: a) the amino group on UiO-66-NH_2 dehydroxylated; b) the amino group on UiO-66-NH_2 hydroxylated; c) the hydroxyl group on UiO-66-NH_2 hydroxylated; d) the hydroxyl group vicinal to the amino group on UiO-66-NH_2 hydroxylated. Positive (blue) and negative (red) regions are reported in the range: -0.069 +0.186 a.u.

In the de-hydroxylated structure, the optimized geometry is characterized by the presence of a hydrogen bond (d($NH^{\cdots}O_{carb}$)=1.962 Å) between the NH_2 group and the oxygen atom that belongs to the carboxylate moiety. Upon adsorption of CO_2 (Figure 6a), the $NH^{\cdots}O_{carb}$ is elongated because of the interaction between the nitrogen atom and CO_2. The CO_2 molecule is located above the amino group with a distance of 2.936 Å between carbon and nitrogen. The B3LYP-D* interaction energy, corrected for the BSSE, is -20.4 kJ/mol per CO_2 molecule. These values are in agreement with previous DFT calculations, by considering that they were performed with a pure GGA functional where the dispersive forces were neglected. In that case, Torrisi et al. reported a $N\cdots CO_2$ distance of 3.1 Å on MIL-53(Al)-NH_2, with an interaction energy of -14.7 kJ/mol.[12]

As mentioned above, three different adsorption sites were considered on the hydroxylated form of UiO-66-NH_2-50. When carbon dioxide is placed such that it interacts with the amino group (i.e. site N), the optimized geometry provides a longer $N\cdots CO_2$ distance (3.107 Å, see Figure 6b) than that on the de-hydroxylated structure. This is because the CO_2 molecule moves slightly so that it can simultaneously interact with the nearby OH

group. In fact, the OH···O=C=O distance amounts to only 2.113 Å. It is worthy to note that because of the distribution of the amino groups in the unit cell, the three molecules are in close contact with each other with a OCO···CO_2 distance of 3.310 Å. This suggests that a self-assembly of carbon dioxide may take place due to the attractive intermolecular quadrupolar-quadrupolar interactions. Note that the intermolecular distance in crystalline CO_2 is 3.107 Å[43], a value not far removed from that observed here. This tendency for self-assembly has been previously observed in other MOFs materials and it is has been reported to be beneficial with respect to adsorption energies.[44] In this case the interaction energy per CO_2 molecule is -34.0 kJ/mol, such that it is the strongest of the adsorption sites under consideration. On the OH site, which resembles the OH group in UiO-66, the CO_2 molecule interacts directly with the hydroxyl group (see Figure 6c) at a distance of 2.003 Å with anunexpectedly high interaction energy of -31.0 kJ/mol. Finally, when the adsorbed molecule interacts directly with the OH vicinal to the amino group (i.e. site $OH_{(NH2)}$), the optimized geometry, as shown in Figure 6d, confirms a tendency of carbon dioxide to self-assemble with the assistance of the hydroxyl group with a OCO···CO_2 distance of 3.152 Å, even closer to the distance observed in crystalline CO_2. The molecule is close to the OH (OH...OCO distance= 2.091 Å) and forms an angle of 150.5° with the hydroxyl group. In contrast, the amino group, at a distance of more than 5 Å from CO_2, is not involved in the interaction. It turns out that the -NH_2 geometry is almost unperturbed. Interestingly, the interaction energy is very close to that of site N with ΔE being -32.8 kJ/mol. This suggests that the interaction with the amino group is also small in the hydroxylated material and that the higher interaction energies observed for the hydroxylated MOF are totally ascribable to the presence of OH groups and not to the NH_2 groups in this structure.

In summary, it is evident that in the hydroxylated structure, the presence of an amino group close to the hydroxyl group leads to an overall stronger interaction than for the OH alone in unfunctionalized UiO-66. The comparison between the hydroxylated and de-hydroxylated structures sheds some light on the role of the OH group. There is a competition between NH_2 and OH, but computed data clearly show that the interaction with CO_2 occurs mainly around the hydroxyl groups. The effect of the two groups (i.e OH and NH_2) increase the binding energy up to 34.0 kJ/mol, in agreement with the experimental results in which a larger q^{diff} was recorded on the amino-functionalized material. Notably, a strengthening of the interaction is likely to occur because of an arrangement of the CO_2 molecules dictated by quadrupolar interactions. Interestingly, the interaction energy of the UiO-66-like OH site is lower than the other sites by about 3 kJ/mol, close to the range of 3-5 kJ/mol observed experimentally. On average, the computed interaction energy is not far from those found experimentally via calorimetric measurements (33 vs 27 kJ/mol). However, the former should be corrected to include the zero-point energy and a thermal correction to enthalpy at T=298K. This contribution has been calculated for the site N structure, amounting to 3.5 kJ/mol. When added to the computed interaction energy, the predicted adsorption enthalpy is -30.5 kJ/mol. If a similar correction is applied to the other modeled adsorption sites, an average value of 29 kJ/mol is obtained, in good agreement with the experiment.

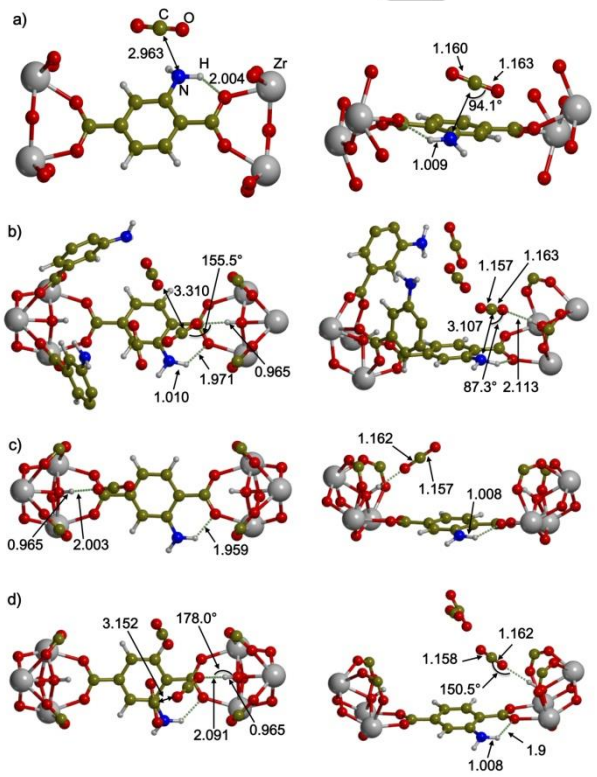

Figure 6. Relevant computed structural features (distances in Å and angles in degrees) of CO_2 in interaction with a) dehydroxylated UiO-66-NH_2; and with different sites of hydroxylated UiO-66-NH_2: b) the amino group (site N); c) the isolated hydroxyl group (site OH); d) the hydroxyl group vicinal to the amino group. Left: top view with respect to the benzene ring; right: side view.

Conclusions

In this work LT- and HT-ML-UiO-66 MOFs coming from two different synthesis methods were investigated towards CO_2

i) FTIR spectroscopy was found to be very useful for the study of solvent removal, a fundamental step before CO_2 adsorption.

ii) Volumetric CO_2 isotherms showed the largest adsorbed CO_2 quantity for UiO-66-NH_2 and the lowest for the unfunctionalised material: from 0.0017 up to 0.0024 mmol/m^2 if normalization to Langmuir surface is performed; The same values are found for both the synthesis procedures when compared with similar NH_2 loading.

iii) Microcalorimetric isotherms revealed that the heat of CO_2 adsorption (q^{diff})was higher in the amino-functionalised materials; the q^{diff} recorded at the lowest equilibrium pressures considered in this study amount to 27 (25) and 20 (22) kJ/mol for HT(LT) UiO-66-NH_2 and UiO-66, respectively.

iv) Ab initio calculations show that in the hydroxylated structure, the presence of one NH_2 group close to the OH group leads to an overall stronger interaction than for the OH alone in the unfunctionalized UiO-66. The combined effect of the two groups

increases the interaction enthalpy to about -29 kJ/mol, a value that is in rather good agreement with the microcalorimetric data.
v) Combining observations from both the experimental and computational data, it is suggested that in order to maximize the sorbate-sorbent interaction between CO_2 and NH_2 functionalized UiO-66 samples, it is crucial to find the optimal activation conditions whereby all the residual solvent is removed while the maximum amount of structural OH groups are preserved.

Experimental Section

Materials

The materials discussed in this study have been synthesized via two different procedures fully described in a recent publication wherein extensive characterization is also provided Ref. [8]. The Mixed ligand MOFs (ML-MOFs) are further divided into two classes: the LT-ML-MOFs prepared at 373K, and HT-ML-MOFs prepared at 493K (see Section A of Supporting Information).

Experimental

In situ FTIR measurements were recorded at room temperature on self-supporting wafers using a Nicolet 6700 FTIR spectrometer equipped with an MCT detector, operating in transmission mode at 2 cm^{-1} resolution. All samples were pretreated under vacuum at 393K for 2 hours (LT-ML-MOFs) and 423K for 1 hour (HT-ML-MOFs) to remove adsorbed solvent molecules. In order to make quantitative comparison of measured intensities, all the spectra have been normalized to the pellet thickness.

CO_2 adsorption isotherms were collected at 298 K on a volumetric instrument (Micromeritics ASAP 2020 sorption analyzer) by use of an isothermal water bath. Prior to analysis, all samples were outgassed on a glass line equipped with a turbomolecular pump for 12 h at room temperature followed by treatment at 393 K (LT-ML-MOFs) or 423 K (HT-ML-MOFs) until the pressure reached $5{\cdot}10^{-4}$ mbar (about 1 h). The samples were then transferred into the analysis cell inside a glove box (M Braun Lab Star Glove Box supplied with pure 5.5 grade Nitrogen, <0.5 ppm O_2, <0.5 ppm H_2O).

The heat of adsorption and the adsorption isotherm were measured simulteniously by means of a C80 microcalorimeter (Calvet type, Setaram, France) and following a well-established stepwise procedure, described in detail elsewhere [21]. This procedure allows for both the integral heats evolved ($-Q^{int}$) and adsorbed amounts (n_{ads}) to be determined in the same experiment for very small increments of the adsorptive pressure. Adsorbed amounts and integral heats evolved, normalized to the unit surface area, were plotted vs pressure in the form of volumetric (quantitative) and calorimetric isotherms, respectively. The adsorption heats observed for each small dose of gas admitted over the sample (q^{diff}) have been finally reported as a function of coverage, in order to obtain the (differential) enthalpy changes associated with the proceeding adsorption process. The differential-heat plots were obtained by taking the middle point of the partial molar heats ($\Delta Q^{int}/\Delta n_{ads}$, kJ/mol) vs n_{ads} histogram relative to the individual adsorptive doses. Before each calorimetric measurement, the samples were activated under vacuum following the same activation procedure adopted for the volumetric measurements. After the first adsorption run the samples were outgassed at 303 K overnight in the calorimeter before performing the second adsorption run, such that the non desorbable (irreversible) adsorbed fraction could be determined.

Modeling

CO_2 adsorption on UiO-66-NH_2 was studied by carrying out periodic density functional theory (DFT) calculations with the hybrid B3LYP functional[22] augmented with an empirical correction term to include dispersive interactions, as proposed by Grimme,[23] with a slight modification for the study of solids.[24] Hereafter, the adopted method is denoted as B3LYP-D*. Calculations were performed by using the CRYSTAL09 program,[25, 26] which has been successfully applied in the study of other MOFs.[27-31] In order to construct a model structure to represent the UiO-66-NH_2-50 sample, an amino group was added to half of the BDC ligands of the UiO-66 unit cell. The resulting unit cell (in both the hydroxylated and de-hydroxylated form) is rhombohedral and belongs to the R3 space group. There are three amino groups per cell.

An all electron basis set of atom centered Gaussian-type functions has been used for Zr, O, N, C and H; namely a *9-7631-621G* basis set for Zr,[15] and a TZP for H, C and N has been adopted.[32] For the numerical integration of the exchange–correlation term, 75 radial points and 974 angular points were adopted in a Lebedev scheme in the region of chemical interest.

The Pack–Monkhorst/Gilat shrinking factors for the k-point sampling of reciprocal space were set to 2 and 2, corresponding to 4 and 4 points at which the Hamiltonian matrix was diagonalized. The accuracy of the integral calculations was increased by setting the tolerances to 7, 7, 7, 7 and 16.

The self-consistent field (SCF) iterative procedure was converged to a tolerance in total energy of $\Delta E = 1 \times 10^{-7}$ a.u. To accelerate convergence in the SCF process, a modified Broyden's scheme following the method proposed by Johnson was adopted.[33, 34] The method was applied after five SCF iterations, with 50% of the Fock/KS matrices mixing and the Johnson's parameter set to 0.05. The above computational parameters ensured a full numerical convergence on all the computed properties described in this work.

Acknowledgements

The Research Council of Norway (CLMIT project no. 215735), VISTA (project no. 6457) and MIUR-PRIN 2010-2011(project n: 2010A2FSS9) are kindly acknowledged for the financial support. We thank Sharmala Aravinthan for her help in materials synthesis and characterization. Improvements of the CRYSTAL code in its massive parallel version were made possible thanks to the PRACE proposals no. 2013081680.

Keywords: Carbon dioxide capture • Metal-organic frameworks • Adsorption • IR spectroscopy • Ab initio calculations

[1] http://www.esrl.noaa.gov/gmd/ccgg/trends/, **2014**.
[2] G. Ferey, C. Serre, T. Devic, G. Maurin, H. Jobic, P. L. Llewellyn, G. De Weireld, A. Vimont, M. Daturi, J. S. Chang, *Chem. Soc. Rev.* **2011**, *40*, 550-562.
[3] K. Sumida, D. L. Rogow, J. A. Mason, T. M. McDonald, E. D. Bloch, Z. R. Herm, T.-H. Bae, J. R. Long, *Chem. Rev.* **2012**, *112*, 724-781.

[4] S. Chaemchuen, N. A. Kabir, K. Zhou, F. Verpoort, *Chem. Soc. Rev.* **2013**, *42*, 9304-9332.
[5] Y. S. Bae, R. Q. Snurr, *Angew. Chem. Int. Ed.* **2011**, *50*, 11586-11596.
[6] S. Couck, J. F. M. Denayer, G. V. Baron, T. Remy, J. Gascon, F. Kapteijn, *J. Am. Chem. Soc.* **2009**, *131*, 6326-6327.
[7] M. Kandiah, M. H. Nilsen, S. Usseglio, S. Jakobsen, U. Olsbye, M. Tilset, C. Larabi, E. A. Quadrelli, F. Bonino, K. P. Lillerud, *Chem. Mater.* **2010**, *22*, 6632-6640.
[8] S. Chavan, G. C. Shearer, S. Svelle, U. Olsbye, F. Bonino, J. Ethiraj, K. P. Lillerud, S. Bordiga, *Inorg. Chem.* **2014**, submitted.
[9] G. E. Cmarik, M. Kim, S. M. Cohen, K. S. Walton, *Langmuir* **2012**, *28*, 15606-15613.
[10] Q. Y. Yang, A. D. Wiersum, P. L. Llewellyn, V. Guillerm, C. Serred, G. Maurin, *Chem. Commun.* **2011**, *47*, 9603-9605.
[11] J. G. Vitillo, M. Savonnet, G. Ricchiardi, S. Bordiga, *ChemSusChem* **2011**, *4*, 1281-1290.
[12] A. Torrisi, R. G. Bell, C. Mellot-Draznieks, *Cryst. Growth Des.* **2010**, *10*, 2839-2841.
[13] J. H. Cavka, S. Jakobsen, U. Olsbye, N. Guillou, C. Lamberti, S. Bordiga, K. P. Lillerud, *J. Am. Chem. Soc.* **2008**, *130*, 13850-13851.
[14] S. Chavan, J. G. Vitillo, D. Gianolio, O. Zavorotynska, B. Civalleri, S. Jakobsen, M. H. Nilsen, L. Valenzano, C. Lamberti, K. P. Lillerud, S. Bordiga, *Phys. Chem. Chem. Phys.* **2012**, *14*, 1614-1626.
[15] L. Valenzano, B. Civalleri, S. Chavan, S. Bordiga, M. H. Nilsen, S. Jakobsen, K. P. Lillerud, C. Lamberti, *Chem. Mater.* **2011**, *23*, 1700-1718.
[16] M. Kim, S. M. Cohen, *CrystEngComm* **2012**, *14*, 4096-4104.
[17] H. Wu, Y. S. Chua, V. Krungleviciute, M. Tyagi, P. Chen, T. Yildirim, W. Zhou, *J. Am. Chem. Soc.* **2013**, *135*, 10525-10532.
[18] S. Biswas, P. Van der Voort, *Eur. J. Inorg. Chem.* **2013**, 2154-2160.
[19] Y. T. Huang, W. P. Qin, Z. Li, Y. W. Li, *Dalton Trans.* **2012**, *41*, 9283-9285.
[20] D. R. Sun, Y. H. Fu, W. J. Liu, L. Ye, D. K. Wang, L. Yang, X. Z. Fu, Z. H. Li, *Chem.-Eur. J.* **2013**, *19*, 14279-14285.
[21] V. Bolis in *Calorimetry and Thermal Methods in Catalysis, Vol. 154* (Ed.: A. Auroux), Springer, Heidelberg, **2013**, pp. 3-50.
[22] A. D. Becke, *J. Chem. Phys.* **1993**, *98*, 5648-5652.
[23] S. Grimme, *J. Comput. Chem.* **2006**, *27*, 1787-1799.
[24] B. Civalleri, C. M. Zicovich-Wilson, L. Valenzano, P. Ugliengo, *CrystEngComm* **2008**, *10*, 405-410.
[25] R. Dovesi, R. Orlando, B. Civalleri, C. Roetti, V. R. Saunders, C. M. Zicovich-Wilson, *Z. Kristallogr.* **2005**, *220*, 571-573.
[26] R. Dovesi, V. R. Sauders, C. Roetti, R. Orlando, C. M. Zicovich-Wilson, F. Pascale, B. Civalleri, K. Doll, N. M. Harrison, I. J. Bush, P. D'Arco, M. Llunell, *CRYSTAL09 2009 User's Manual.* **2009**, University of Torino, Torino.
[27] B. Civalleri, F. Napoli, Y. Noel, C. Roetti, R. Dovesi, *CrystEngComm* **2006**, *8*, 364-371.
[28] L. Valenzano, B. Civalleri, K. Sillar, J. Sauer, *J. Phys. Chem. C* **2011**, *115*, 21777-21784.
[29] A. M. Walker, B. Civalleri, B. Slater, C. Mellot-Draznieks, F. Cora, C. M. Zicovich-Wilson, G. Roman-Perez, J. M. Soler, J. D. Gale, *Angew. Chem. Int. Ed.* **2010**, *49*, 7501-7503.
[30] E. Albanese, B. Civalleri, M. Ferrabone, F. Bonino, S. Galli, A. Maspero, C. Pettinari, *J. Mater. Chem.* **2012**, *22*, 22592-22602.
[31] G. C. Shearer, V. Colombo, S. Chavan, E. Albanese, B. Civalleri, A. Maspero, S. Bordiga, *Dalton Trans.* **2013**, *42*, 6450-6458.
[32] A. Schafer, H. Horn, R. Ahlrichs, *J. Chem. Phys.* **1992**, *97*, 2571-2577.
[33] C. G. Broyden, *Math. Comput* **1965**, *19*, 557–593
[34] D. D. Johnson, *Phys. Rev. B* **1988**, *38*, 12807-12813.
[35] S. F. Boys, F. Bernardi, *Mol. Phys.* **1970**, *19*, 553-566.
[36] G. C. Shearer, S. Forselv, S. Chavan, S. Bordiga, K. Mathisen, M. Bjorgen, S. Svelle, K. P. Lillerud, *Top. Catal.* **2013**, *56*, 770-782.
[37] S. R. Caskey, A. G. Wong-Foy, A. J. Matzger, *J. Am. Chem. Soc.* **2008**, *130*, 10870-10871.
[38] B. Bonelli, B. Civalleri, B. Fubini, P. Ugliengo, C. O. Arean, E. Garrone, *J. Phys. Chem. B* **2000**, *104*, 10978-10988.
[39] Q. Y. Yang, A. D. Wiersum, H. Jobic, V. Guillerm, C. Serre, P. L. Llewellyn, G. Maurin, *J. Phys. Chem. C* **2011**, *115*, 13768-13774.
[40] A. D. Wiersum, E. Soubeyrand-Lenoir, Q. Y. Yang, B. Moulin, V. Guillerm, M. Ben Yahia, S. Bourrelly, A. Vimont, S. Miller, C. Vagner, M. Daturi, G. Clet, C. Serre, G. Maurin, P. L. Llewellyn, *Chem.-Asian J.* **2011**, *6*, 3270-3280.
[41] J. Gascon, M. D. Hernandez-Alonso, A. R. Almeida, G. P. M. van Klink, F. Kapteijn, G. Mul, *ChemSusChem* **2008**, *1*, 981-983.
[42] G. Shearer, S. Chavan, J. Ethiraj, J. G. Vitillo, S. Svelle, U. Olsbye, C. Lamberti, S. Bordiga, K. P. Lillerud, *Chem. Mater.* **2014**, doi: 10.1021/cm501859p.
[43] A. Simon, K. Peters, *Acta Cryst. B* **1980**, *36*, 2750-2751.
[44] S. C. Xiang, Y. B. He, Z. J. Zhang, H. Wu, W. Zhou, R. Krishna, B. L. Chen, *Nat. Commun.* **2012**, *3*, 954.

Table of Contents

FULL PAPER

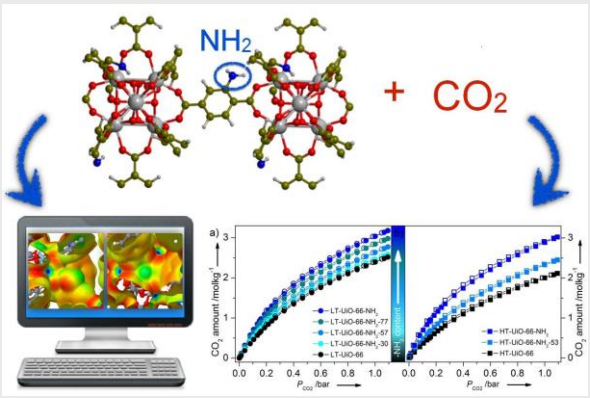

A series of mixed ligand UiO-66 MOFs, synthesized via two different methods have been investigated for their CO_2 adsorption properties from 0 to 1 bar in order to clarify the role of NH_2 loading on CO_2 uptake.

Jayashree Ethiraj,[a] Elisa Albanese, [a] Bartolomeo Civalleri, [a] Sachin Chavan, [b] Greig C. Shearer,[b] Karl Petter Lillerud,[b] Silvia Bordiga,[a] Jenny G. Vitillo,[a,c] Francesca Bonino*[a]*

Page No. – Page No.

CO_2 Adsorption in Amine Functionalized Mixed Ligand Metal-organic Frameworks of UiO-66 topology

Supporting Information

A) Synthesis of LT/HT-MOFs

LT-ML-MOFs (low temperature mixed ligand metal organic frameworks) and HT-ML-MOFs (high temperature mixed ligand metal organic frameworks).

For LT-ML-MOFs, once all the reagents (N,N-dimethylformamide, $ZrCl_4$, H_2O, and linker) were sequentially introduced in a volumetric flask, this was sealed and placed in an oven at 100 °C for 72 hours. The resulting microcrystalline powders were washed three times in DMF, three times in excess of water at 80 °C for 2 hours and dried at 60 °C in air for 24 hours. In order to obtain materials with varying extent of amino functionality, five different 2-amino-1,4-benzenedicarboxylic acid (ABDC) to 1,4-benzenedicarboxylic acid (BDC) molar ratios were used; 0, 0.25, 0.50, 0.75 and 1.00. The five materials so obtained were denominated LT-UiO-66, LT-UiO-66-NH_2-30, LT-UiO-66-NH_2-57, LT-UiO-66-NH_2-77, and LT-UiO-66-NH_2, respectively according to the percentage amino loading in the final product (determined via dissolution/^{1}H NMR, ref. [1]).

The HT-ML-MOFs were synthesized via a method which limits the number of missing linker defects in the material. $ZrCl_4$ and linker (BDC and/or ABDC) were dissolved separately in different portions of DMF. HCl was introduced to the flask designated to $ZrCl_4$ after the addition of DMF but prior to the addition of metal salt. The two solutions were mixed and transferred to 200 ml Teflon-lined autoclaves where they were heated to 220 °C for 20 hours under static conditions. The powder precipitates were filtered, washed in boiling water and dried at 60 °C in air. For a direct comparison with the previous series, only three of the resulting materials have been taken into account: HT-UiO-66, HT-UiO-66-NH_2-53, HT-UiO-66-NH_2.

B) Modelling of FTIR spectra

Vibrational frequencies at the Γ point and their IR intensities were calculated on the optimized geometries for the bare MOF by means of a mass-weighed Hessian matrix, obtained by numerical differentiation of the analytical first derivatives.[2, 3]

An anharmonic correction was performed on the OH and NH stretching modes. [4, 5] The automated procedure is the following: (i) the O—H and N—H distances have been assumed as a normal coordinate decoupled with respect to all other modes; (ii) the total energy of the system for a set of OH and NH values around equilibrium (-0.2/ 0.25 Å) have been calculated; (iii) a polynomial curve of sixth degree was used to best fit the energy points; (iii) the one-dimensional nuclear Schrödinger equation was solved to obtain the three lowest

eigenvalues E0, E1 and E2 from which the fundamental frequencies $\omega_{01} = E_1 - E_0$, the first overtone $\omega_{02} = E_2 - E_0$ and the anharmonicity constants of the OH and NH modes, $\omega_e\chi_e = (2\omega_{01} - \omega_{02})/2$ were calculated.

Both hydroxylated and dehydroxylated forms of UiO-66-NH_2 were modeled. An amino group was added to half of the BDC ligands of the unit cell, in order to simulate a hypothetically regular UiO-66-NH_2-50 sample. Figure S1 compares the experimental and simulated IR spectrum obtained on LT-UiO-66-NH_2-57 and (the hypothetical) UiO-66-NH_2-50 respectively. In the NH stretching region, two peaks are clearly observed, due to asymmetric and symmetric vibrations of NH_2 functional groups. For a better comparison between the computed and experimental IR spectra, an estimated anharmonic correction of 150 and 122 cm^{-1} was applied to the OH and NH stretching modes, respectively, while frequencies in the 3300-1000 cm^{-1} range were uniformly scaled by a factor 0.98. In addition, a larger FHWH was used for the NH stretching modes to take into account the broadening of the corresponding peaks due to the H-bonding interaction of the NH_2 group with the oxygen of the carboxylate.

The resulting simulated spectrum nicely agrees with that obtained experimentally. The OH and NH stretching regions fit particularly well with the model, such that a semi-quantitative agreement is observed, allowing the three bands to be unambiguously assigned to one OH stretch and two NH stretching modes. Notably, the computed results confirm that the amino groups are hydrogen bonded with one of the oxygens of the nearby carboxylate moiety. In addition, computed data confirm that the peak around 1019 cm^{-1} is characterized by modes due to the C-H deformation of the linkers without the amino groups, as for UiO-66, while the new bands around 1050 and 980 cm^{-1} are C-H deformations coupled with N-H modes in the ABDC linkers. It turns out that the intensity of the band at 1019 cm^{-1} decreases as observed experimentally.

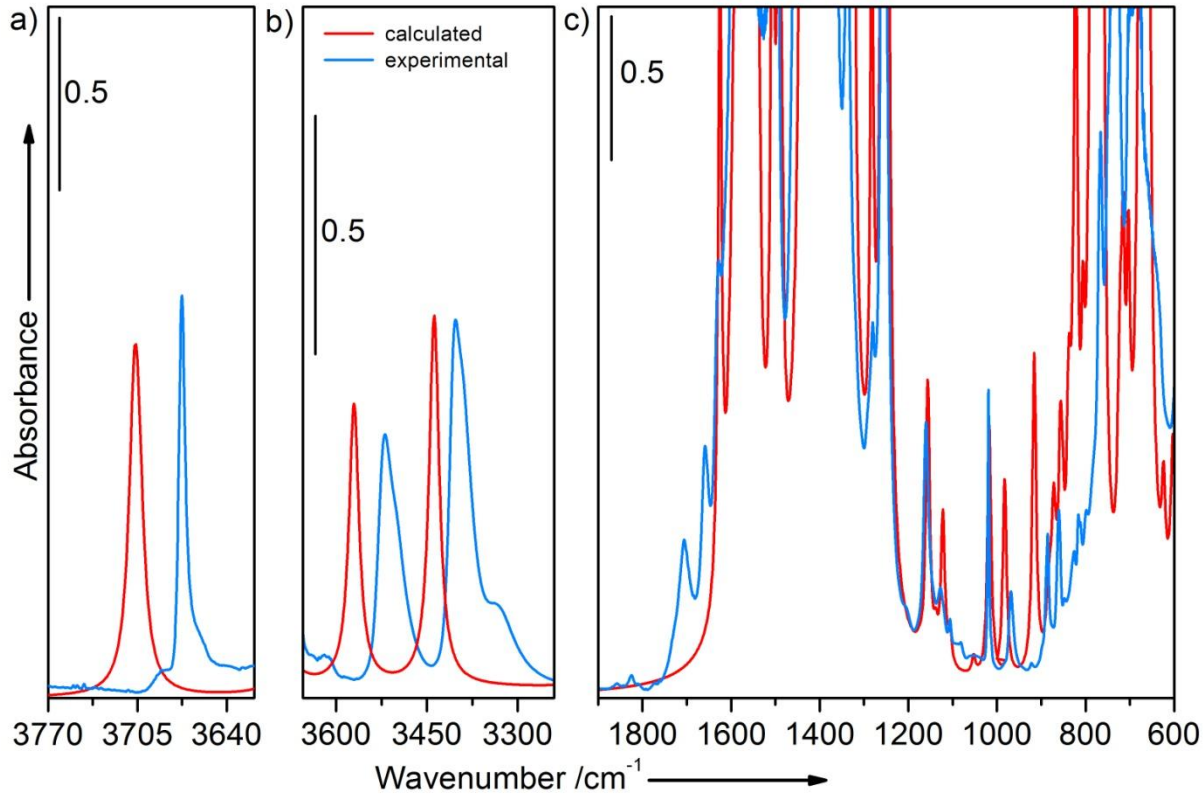

Figure S1. Simulated (red) and experimental (light blue) FTIR spectra of hydroxylated UiO-66-NH_2-50 and LT-UiO-66-NH_2-57, respectively. The spectra are divided into three regions: a) the OH stretching region; b) the NH_2 stretching region; and c) the framework mode region. The simulated OH and NH modes have been scaled by the computed anharmonic factor (see text), while the frequencies in the range 3300-1000 cm^{-1} are scaled by a factor of 0.98 to best fit the experimental IR spectra. The simulated spectrum has been computed using a Lorentzian function with a FWHM of 20 cm^{-1} for NH stretching modes and 10 cm^{-1} for all the others.

C) FT-IR spectroscopic study of CO_2 adsorption on MOFs

In situ FTIR measurements of CO_2 adsorption were recorded at room temperature on self-supporting wafers using a Nicolet 6700 FTIR spectrometer equipped with an MCT detector, operating in transmission mode at 2 cm^{-1} resolution. Gas phase CO_2 was dosed such that $P_{eq}(CO_2)$ was 30 mbar, and spectra were recorded while the pressure in the IR cell was progressively reduced.

The main spectral feature observed in Figure S2b is an intense band centered at 2339 cm^{-1}, assigned to the asymmetric stretching mode (ν_3) of adsorbed CO_2. Although this mode is red shifted of 10 cm^{-1} with respect to that observed in gas phase CO_2 (ν_3=2349.3 cm^{-1}), this shift, observed in many MOFs and zeolites [6-10], is essentially due to the confinement effect that the material pore structure imparts on the molecule, an effect which is absent in the free gas.[9]

In all cases, the low adsorption energy was confirmed by the complete reversibility of the CO_2 adsorption process, as evident on the spectra reported in Figure S2b, where the band at 2339 cm^{-1} is progressively eroded upon outgassing at RT. Furthermore, the very weak interaction of CO_2 with the NH_2 and OH groups is confirmed by the fact that their respective stretching modes are completely unperturbed, even at the highest CO_2 dosage (see Figure S2a). These findings were fully confirmed by the calorimetric measurements.

The remarkable result is that it is always the same, independent of the content of NH_2 functional groups in the material or whether synthesized with the LT or HT synthesis methods, even though structural and chemical differences have been evidenced for these materials in a previous study.[1] This observation seems to indicate that IR spectroscopy is not a sensitive method to characterize CO_2 adsorption in materials without strongly interactive sites, the reason being that its vibrational modes are not sensitive to any interaction which the molecule may have. These findings are in agreement with previous computational work. [9]

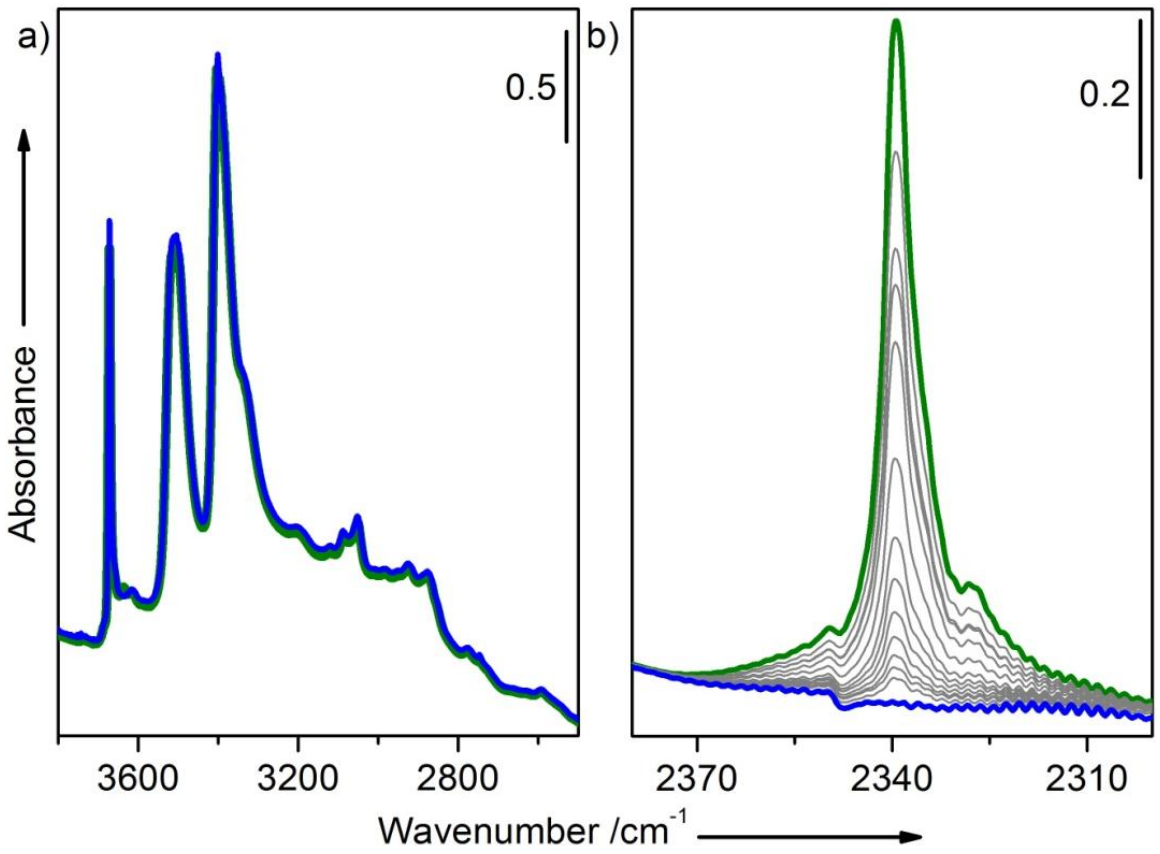

Figure S2. FT-IR spectra of CO_2 adsorption on LT-UiO-66-NH_2 MOF: a) OH and NH_2 stretching region, and b) asymmetric CO_2 stretching range. Blue and green curves were obtained on the activated material before and after sending 30 mbar of CO_2, respectively. Gray spectra report intermediate CO_2 coverages.

D) Calculation of simulated adsorption isotherms for N_2 adsorption in UiO-66-NH_2 at 77K

Adsorption isotherms are calculated with the "Sorption tool" in Accelrys Materials Studio version 7.01. The adsorptive is a geometry optimized N_2 molecule at 77 K. The method is set to Metropolis, which uses COMPASS force field and charges are force field assigned. Summation methods used; electrostatic is Ewald & group based while van der Waals forces are calculated atom based. No constraints are assigned. The isotherms are calculated from 0.1 to 100 kPa with 50 fugacity steps distributed logarithmically to have more points in the steep initial portion of the isotherm. The overall quality was calculated with both "Normal" and "Fine" settings. The "Normal" setting uses 10,000 equilibration steps and 100,000 production steps while the "Fine" setting uses 100,000 equilibration steps and 1,000,000 production steps. Using the "Fine" settings invariably provides a higher calculated surface area due to

the fact that there are more attempts to add a new nitrogen molecule. Due to the statistical nature of the calculations, there a small spread observed in the calculated values when they are repeated. Brunauer-Emmett-Teller (BET) surface areas were calculated from the simulated isotherms by fitting them in the p/p_0 range 0 – 0.1.

Replacement of the hydrogen atom with a NH_2 group take up space in the cavities but not a lot. The number of N_2 molecules adsorbed per unit cell is reduced form 84(83) to 80 when a comparison is done with regular UiO-66 and UiO-66-NH_2. There are 4 octahedral and 8 tetrahedral cages per unit cell. So one less N_2 molecule can fit the octahedral cage when the NH_2 groups are present. Highly symmetrical version of UiO-66-NH_2 in PM-3 is used.

Calculated BET surface area from the simulated isotherms gives 1125 m^2/g for UiO-66 and 1016 m^2/g for UiO-66-NH_2, with a difference of 109 m^2/g. Half of the difference is due to less space the other half is due to higher density. The uncertainty in the calculated values are at least +/-20 m^2/g. (+/- one N_2 molecule).

Measured values for the materials synthesized at higher temperature are 1170 m^2/g and 1057 m^2/g for UiO-66 and UiO-66-NH_2 respectively, with a difference 114 m^2/g.

The two set of data are quite in agreement.

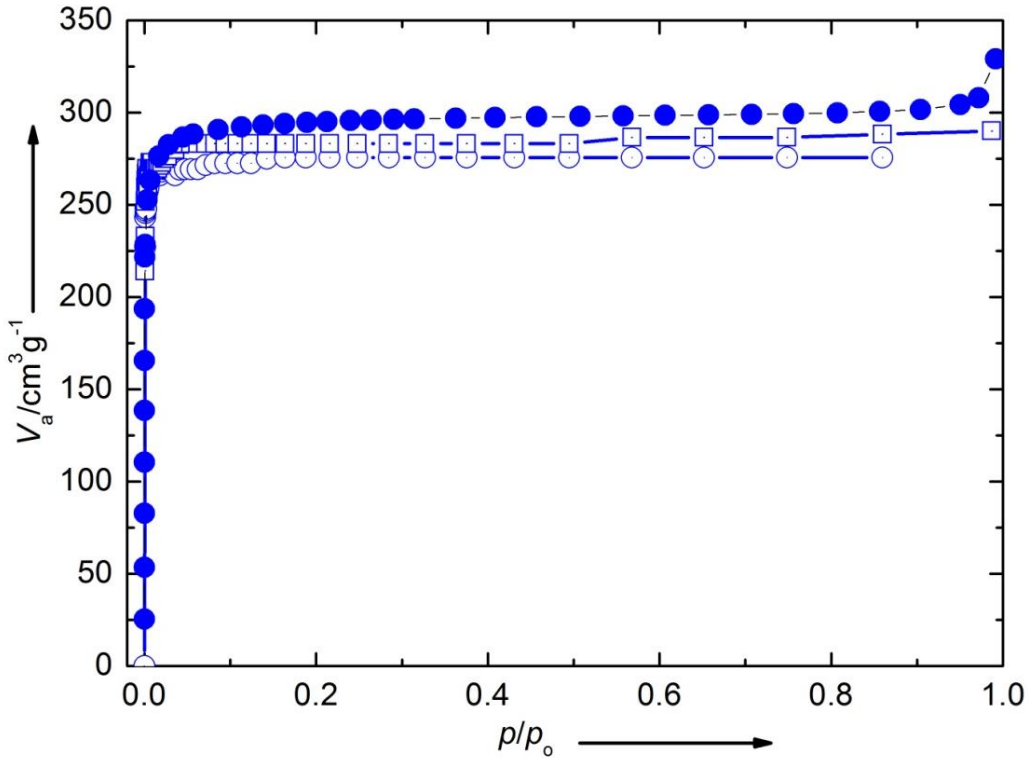

Figure S3. Comparison of measured (filled symbols) and calculated (open symbols) adsorption isotherms for UiO-66 NH_2. The two isotherms with open symbols are calculations with identical settings but since this is based on statistical methods will there be small

deviations in the results. There is an uncertainty that corresponds to ± one N_2 molecule per cage. The correspondence with measured isotherm for HT-UiO-66 (full symbols) is very good. A slightly higher absorption in the measured isotherm is probably due to a small amount of defects (missing linkers) also in the material synthesized at 220 °C.

E) PXRD of LT/HT ML-MOFs after the CO_2 adsorption volumetric isotherms

X-ray Powder Diffraction (XRPD) patterns have been collected with a PW3050/60 X'Pert PRO MPD diffractometer from PANalytical working in Debye–Scherrer geometry, using as source the high power ceramic tube PW3373/10 LFF with a Cu anode equipped with Ni filter to attenuate Kb and focused by X-ray mirror PW3152/63. Scattered photons have been collected by a RTMS (Real Time Multiple Strip) X'celerator detector. The samples have been measured as powders inside a 0.8 mm boronsilicate capillary filled in a glove-box and sealed in inert atmosphere, in order to prevent contamination from moisture.

All the series of LT-ML-MOFs and HT-ML-MOFs are isostructural with respect to UiO-66. In figure a1) and a2), the lower angle peaks in the 2θº range of 2-10 show that the porosity of the samples are preserved in both LT-ML-MOFs and HT-ML-MOFs.

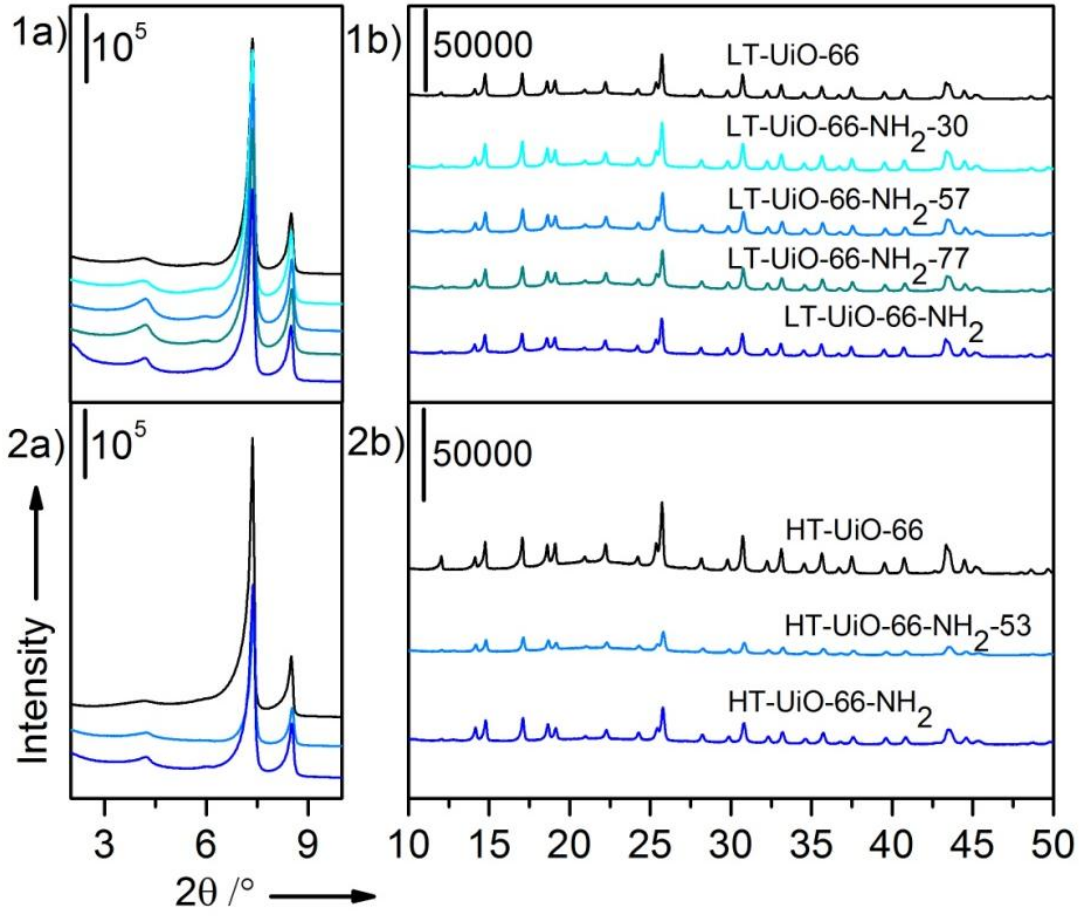

Figure S4. PXRD of LT-ML-MOFs 1) and HT-ML-MOFs 2) after the CO_2 adsorption volumetric isotherms. Parts a): small angles. Parts b): higher angles.

References

[1] S. Chavan, G. C. Shearer, S. Svelle, U. Olsbye, F. Bonino, J. Ethiraj, K. P. Lillerud, S. Bordiga, *Inorg. Chem.* **2014**, submitted.

[2] F. Pascale, C. M. Zicovich-Wilson, F. L. Gejo, B. Civalleri, R. Orlando, R. Dovesi, *J. Comput. Chem.* **2004**, *25*, 888-897.

[3] C. M. Zicovich-Wilson, F. J. Torres, F. Pascale, L. Valenzano, R. Orlando, R. Dovesi, *J. Comput. Chem.* **2008**, *29*, 2268-2278.

[4] M. Mérawa, B. Civalleri, P. Ugliengo, Y. Noël, A. Lichanot, *J. Chem. Phys.* **2003**, *119*, 1045-1052.

[5] M. Mérawa, P. Labéguerie, P. Ugliengo, K. Doll, R. Dovesi, *Chem. Phys. Lett.* **2004**, *387*, 453-459.

[6] A. Vimont, A. Travert, P. Bazin, J. C. Lavalley, M. Daturi, C. Serre, G. Ferey, S. Bourrelly, P. L. Llewellyn, *Chem. Commun.* **2007**, 3291-3293.

[7] B. Bonelli, B. Civalleri, B. Fubini, P. Ugliengo, C. O. Arean, E. Garrone, *J. Phys. Chem. B* **2000**, *104*, 10978-10988.

[8] G. C. Shearer, V. Colombo, S. Chavan, E. Albanese, B. Civalleri, A. Maspero, S. Bordiga, *Dalton Trans.* **2013**, *42*, 6450-6458.

[9] J. G. Vitillo, M. Savonnet, G. Ricchiardi, S. Bordiga, *ChemSusChem* **2011**, *4*, 1281-1290.

[10] M. Kandiah, M. H. Nilsen, S. Usseglio, S. Jakobsen, U. Olsbye, M. Tilset, C. Larabi, E. A. Quadrelli, F. Bonino, K. P. Lillerud, *Chem. Mater.* **2010**, *22*, 6632-6640.